Trends and variability in column-integrated atmospheric water vapor

Article *in* Climate Dynamics · June 2005

DOI: 10.1007/s00382-005-0017-4

3 authors, including:

John T Fasullo
National Center for Atmospheric Research
119 PUBLICATIONS **19,821** CITATIONS

Climate Dynamics (2005) 24: 741–758
DOI 10.1007/s00382-005-0017-4

Kevin E. Trenberth · John Fasullo · Lesley Smith

Trends and variability in column-integrated atmospheric water vapor

Received: 06 December 2004 / Accepted: 14 February 2005 / Published online: 11 May 2005

Abstract An analysis and evaluation has been performed of global datasets on column-integrated water vapor (precipitable water). For years before 1996, the Ross and Elliott radiosonde dataset is used for validation of European Centre for Medium-range Weather Forecasts (ECMWF) reanalyses ERA-40. Only the special sensor microwave imager (SSM/I) dataset from remote sensing systems (RSS) has credible means, variability and trends for the oceans, but it is available only for the post-1988 period. Major problems are found in the means, variability and trends from 1988 to 2001 for both reanalyses from National Centers for Environmental Prediction (NCEP) and the ERA-40 reanalysis over the oceans, and for the NASA water vapor project (NVAP) dataset more generally. NCEP and ERA-40 values are reasonable over land where constrained by radiosondes. Accordingly, users of these data should take great care in accepting results as real. The problems highlight the need for reprocessing of data, as has been done by RSS, and reanalyses that adequately take account of the changing observing system. Precipitable water variability for 1988–2001 is dominated by the evolution of ENSO and especially the structures that occurred during and following the 1997–98 El Niño event. The evidence from SSM/I for the global ocean suggests that recent trends in precipitable water are generally positive and, for 1988 through 2003, average 0.40 ± 0.09 mm per decade or $1.3 \pm 0.3\%$ per decade for the ocean as a whole, where the error bars are 95% confidence intervals. Over the oceans, the precipitable water variability relates very strongly to changes in SSTs, both in terms of spatial structure of trends and temporal variability (with a regression coefficient for 30°N–30°S of 7.8% K^{-1}) and is consistent with the assumption of fairly constant relative humidity. In the tropics, the trends are also influenced by changes in rainfall which, in turn, are closely associated with the mean flow and convergence of moisture by the trade winds. The main region where positive trends are not very evident is over Europe, in spite of large and positive trends over the North Atlantic since 1988. A much longer time series is probably required to obtain stable patterns of trends over the oceans, although the main variability could probably be deduced from past SST and associated precipitation variations.

The National Center for Atmospheric Research is sponsored by the National Science Foundation.

K. E. Trenberth (✉) · J. Fasullo · L. Smith
National Center for Atmospheric Research, Boulder, CO80307 USA
E-mail: trenbert@ucar.edu
Tel.: +1-303-4971318
Fax: +1-303-4971333

1 Introduction

Water vapor plays a major role in climate as a dominant feedback variable in association with radiative effects and moist dynamics. In the lower troposphere, water vapor in the atmosphere acts as the main resource for precipitation in all weather systems, providing latent heating in the process and dominating the structure of diabatic heating in the troposphere (Trenberth and Stepaniak 2003a, b). Trenberth (1999) estimates that, for extratropical cyclones, on average about 70% of the precipitation comes from moisture that was already in the atmosphere at the time the storm formed, while the rest comes from surface evaporation, or more generally evapotranspiration, during the course of the storm's evolution. As climate warms, the amount of moisture in the atmosphere, which is governed by the Clausius–Clapeyron equation, is expected to rise much faster than the total precipitation amount, which is governed by the surface heat budget through evaporation (Trenberth et al. 2003). This means that storms will be affected and it implies that the main changes to be experienced are in the character of precipitation: increases in intensity must be offset by decreases in duration or frequency of events,

or perhaps by changes in efficiency, as well as changes in phase from snow to rain. Such changes are observed in the United States (Groisman et al. 2004). Increased intensity of precipitation further implies stronger latent heating and increasing intensity of weather systems. At the extremes of precipitation incidence are the events that give rise to floods and droughts, whose changes in occurrence and severity have enormous impact on the environment and society. Changes in water vapor amounts are, therefore, key determinants of climate change character.

In addition, water vapor is the most important greenhouse gas (Kiehl and Trenberth 1997). Its changes in the upper troposphere are especially important for climate change (Held and Soden 2000), but are poorly known. Some changes in water vapor in the upper troposphere stem directly from human influences through emissions from aircraft and associated generation of contrails, and these contribute to radiative forcing of order 0.1 W m^{-2} that is expected to grow in time but is not well measured (Marquart et al. 2003). Of course as water vapor condenses into clouds, other radiative effects become important and clouds are the greatest source of uncertainty in climate models.

Hence, advancing the understanding of variability and change in water vapor is vital, but knowledge is limited by inadequate observations. In this paper, we assess changes in atmospheric water vapor, with a focus on the column-integrated amount, known as precipitable water. We are especially interested in evaluating and exploiting the ERA-40 reanalysis data from the European Centre for Medium range Weather Forecasts (ECMWF), see Uppala et al. (2005). We also use the National Centers for Environmental Prediction/National Center for Atmospheric Research (NCEP/NCAR) (henceforth NCEP-1) (Kalnay et al. 1996) and NCEP-2 (Kanamitsu et al. 2002) reanalyses. Other global analyses of water vapor fields are part of the NASA water vapor project (NVAP) dataset (Randel et al. 1996), which we also use. Over land, radiosonde data from Ross and Elliott (1996, 2001) provide direct measurements for possible validation. Over the oceans after mid-1987, precipitable water analyses are available from the special sensor microwave imager (SSM/I). Specifically, products from remote sensing systems (RSS, see Liu et al. 1992; Wentz 1997), which uses the Wentz algorithm, are used. The datasets are described in more detail in Sect. 2.

From carefully quality-controlled observations, it appears that atmospheric moisture amounts generally increased in the atmosphere after about 1973 (prior to which reliable moisture soundings are mostly not available) through 1995 (Ross and Elliott 2001). Hense et al. (1988) revealed increases in moisture over the western Pacific. In the Western Hemisphere north of the equator, annual mean precipitable water amounts below 500 hPa increased over the United States, Caribbean and Hawaii by about 5% per decade revealing a statistically significant trend from 1973 through 1993 (Ross and Elliott 1996), and these correspond to significant increases of 2–3% per decade in relative humidities over the Southeast, Caribbean and subtropical Pacific. Most of the increase is, however, related to temperature and hence in atmospheric water-holding capacity. In China, analysis by Zhai and Eskridge (1997) also revealed upward trends in precipitable water in all seasons and for the annual mean from 1970 to 1990. Precipitable water and relative humidities did not increase over much of Canada, and decreases were evident where temperatures declined in northeast Canada (Ross and Elliott 1996).

Ross and Elliott (2001) extended their regional analysis of sonde data to the northern hemisphere. They confirm the generally upward trends in precipitable water for 1973–1995 over China and southern Asia, strong upward trends in the tropical Pacific, but found small and insignificant trends over Europe. We have obtained the Ross and Elliott (2001) radiosonde results to use as validation where possible. However, major changes in radiosonde types at the end of 1995 (Elliott et al. 2002) and more recently have made further updates of those analyses difficult. We update six coastal stations in the U.S. through 1999.

One global constraint on vertically integrated water vapor amounts is due to conservation of mass. The global mean surface pressure from water vapor changes should match those of actual surface pressure, as this is the only significant influence on global mass within measurement accuracies. Trenberth and Smith (2005) document changes in global surface pressure, water vapor surface pressure and dry air surface pressure from ERA-40, ERA-15 and NCEP-1 reanalyses. Considerable problems are evident prior to 1979, but results are quite good thereafter for ERA-40, with a standard error in monthly global surface pressure anomalies of 0.035 hPa while real fluctuations often exceed ± 0.1 hPa. Results are not as good for NCEP-1. There is an increase in global water vapor amount with El Niño, although the main increase is in the equatorial region from 10°N to 20°S often with compensating drier regions near 20°N. During the 1982–1983 and 1997–1998 El Niño events, global mean water vapor amounts and total mass increased by about 0.1 hPa in surface pressure for several months. For the latter event, the result is reproduced in global surface pressure and in NCEP-1 reanalyses, providing strong evidence that it is real. Trenberth and Smith (2005) show that some evidence exists for slight decreases following the Mount Pinatubo eruption in 1991, as also found by Soden et al. (2002), and also for upward trends associated with increasing global mean temperature, partially verified by upward trends in surface pressure. The least-squares linear trends from September 1985 to August 2002 are 0.12 hPa per decade for the global analyzed surface pressure and 0.09 hPa per decade for the contribution derived from humidity. As this comes from the analysis of observations, it likely has a real basis. However, as uncer-

tainties due to the changing observing system compromise the evidence, these aspects are explored much more here.

In this paper, to extend the Ross and Elliott (2001) results both in time and over the oceans, we focus on the trends after 1988 when SSM/I data are available. Records from a few radiosonde stations where the type of sonde has not changed are also extended. As we will see, the various products have very different trends but they also have some variability in common. We designed an analysis to bring out the common aspects and in the process determined that only one product, the SSM/I from RSS, is really credible, as the others have significant identifiable problems. Accordingly, the material presented reflects also the results of the evaluation. Section 2 describes the datasets and methods in more detail. Section 3 presents the results, firstly with a detailed comparison of ERA-40 with Ross and Elliott (2001) radiosonde results for 1973–1995, and some comparisons of NVAP with Ross and Elliott (2001) data. Some results are extended through 2003 and results for six U.S. radiosonde stations are presented through 1999. This is followed by an analysis of trends, variability and differences among the datasets over 1988–2001, and then empirical orthogonal function (EOF) analyses results. The discussion and conclusions are given in Sect. 4.

2 Datasets and methods

The datasets used in this study are the ERA-40 reanalyses, the NCEP-1 and NCEP-2 reanalyses, SSM/I, NVAP, and the radiosondes from Ross and Elliott, with an update from the NCEP archive created by Jack Woollen at a few stations through 1999. Unfortunately, there is no good standard that can be used to calibrate or validate results. The main historical observations of water vapor have come from radiosondes after about 1945. Quite aside from the limited spatial distribution and only up to twice-daily soundings, the biggest shortcoming has been the moisture sensor and its changes over time; summaries for the U.S. are given by Elliott and Gaffen (1991) and Trenberth (1995; see his Table 1) and updated in Elliott et al. (2002). Fairly crude sensors were used in early radiosondes that suffered from slow response times and biases. In the U.S. a carbon humidity element was introduced in 1965, but low relative humidities (below 20%) were not reported until after 1993. Limits were also applied to high humidities (values in clouds were set at 95%). Shortcomings of operational sondes are well known (e.g., Ross and Elliott 2001; Guichard et al. 2000; Wang et al. 2002; Lanzante et al. 2003). A prototype reference sonde developed by NCAR (Wang et al. 2003) was extensively tested against operational Vaisala and VIZ sondes during IHOP, the International Water Vapor (H_2O) Program, in the central United States during a field program in the summer of 2002. It further revealed the poor performance of operational sondes at temperatures below about −20°C while measuring humidity. Accordingly, Ross and Elliott (1996, 2001) have used water vapor only up to 500 hPa in their analyses of sonde data. In addition, the major changes in U.S. radiosonde types at the end of 1995 (Elliott et al. 2002) led to spurious changes that depend on time of observation, elevation, location, and season. In terms of moisture, there was a spurious drying but mainly in the upper troposphere. In the lower troposphere, the relative humidity decreased from 5% to 8% with the switch from VIZ to Vaisala sondes. For radiosondes, missing data can also be a substantial concern.

We use the Version-5 precipitable water analyses from RSS SSM/I from a series of six intercalibrated satellites (F08, F10, F11, F13, F14, and F15) combined when they overlap, see Wentz (1997). The RSS record has been revised through several versions, and an evaluation by Sohn and Smith (2003) used the Wentz algorithm as the standard and outlined reasons why there are many algorithms applied to SSM/I data and why they differ. All of the DMSP satellites were launched into a near circular subsynchronous polar orbit. Except for F10, this was achieved and the equator crossing time changed by less than an hour over the lifetime of the mission. The exception is F10, which did not achieve the desired orbit and the equator crossing time increased from 19:42 at launch on 1 December 1990 to 22:09 in September 1995, a change of 2 h 27 min. Accordingly, an allowance has to be made for diurnal cycle drift in the record of F10. In addition, the ascending equator crossing times varied from 06:15 for F8, to 17:42 for F13, 18:11 for F11, 19:42 for F10, 20:21 for F14, and 21:31 for F15. Therefore adjustments have to be made for the diurnal cycle. RSS has paid careful attention to cross calibration across different satellites in their Version-5 (http://www.ssmi.com/ssmi/ssmi_description.html) that "allows investigators to confidently use the SSM/I products for detailed interannual and decadal trends studies". We further explore the effects of cross calibration on trends in Sect. 3.4. All algorithms depend on calibration with radiosonde records and thus build in any biases from the latter.

An alternative algorithm from Greenwald and Stephens (GS, Greenwald et al. 1993) applied to SSM/I data has been incorporated in the global NVAP (Randel et al. 1996) dataset. An evaluation of early versions of these two algorithms found deficiencies in the GS product (Trenberth and Guillemot 1995). Since that evaluation, both NVAP and RSS SSM/I records have continued and further issues arise from how records from instruments on successive satellites are merged, especially in the NVAP dataset (Von der Haar et al. 2003). Major changes in processing procedures occurred beginning in 1993, with the introduction of the 22 GHz SSM/I channel, and in 2000 with a "next generation" processing system involving multiple changes. Simpson et al. (2001) explored the time-dependent biases of the

NVAP dataset and noted a discontinuity at the beginning of 1993 associated with the change in procedures.

We use the NCEP-1 reanalyses (Kalnay et al. 1996) in model (sigma) coordinates at full resolution, thereby avoiding any errors from interpolating into pressure surfaces and allowing exact vertical integrals to be computed. These reanalyses did not assimilate SSM/I water vapor data or utilize the water vapor infrared channels. Trenberth and Guillemot (1998) evaluated NCEP-1 reanalysis for water vapor and found substantial problems, with bulls eyes around isolated island stations, indicating a strong model influence, and biases over much of the oceans. The goal of NCEP-2 (Kanamitsu et al. 2000) was to improve upon the NCEP-1 reanalysis by fixing some errors and by updating the parameterizations of the physical processes. However, the data stream was the same and the changes did not greatly affect water vapor. Zveryaev and Chu (2003) analyzed the precipitable water record from NCEP-1 for 1979–1998 and also from 1948 to 1998 and found that the dominant pattern of variability featured spurious trends associated with changes in the observing system.

For ERA-40, a full description is given by Uppala et al. (2005). From 1979 onwards, ERA-40 bias-corrected the radiosonde data to account for at least part of the radiation errors (Andrae et al. 2004). Corrections of up to 2°C in magnitude evolved with time as sondes changed and were devised as a function of sun elevation angle, although the largest corrections are applied in the stratosphere. Nevertheless, the almost universal need to make such corrections and the evidence of improved rms departures from the first guess fields demonstrate the lack of an adequate baseline to calibrate results. The ERA-40 data, we use, is at T106 resolution (1.125°) although most analysis is at T63 resolution. In all cases of reduced resolution, a taper is applied near the truncation limit to greatly reduce any ringing effects.

For ERA-40, SSM/I radiances are assimilated as brightness temperatures and a retrieval is effectively performed that makes use of other variables (surface wind stress is needed, for instance). The resulting product makes use of all other observations as well. A major advantage of ERA-40 is that it applies the data at the time of observation, thereby avoiding possible problems associated with orbital drift, different time of day of observations, and aliasing of the diurnal cycle. These reanalyses also make use of water vapor channels from TIROS operational vertical sounder (TOVS) and ATOVS as well as SSM/I radiances, which should have a substantial positive influence over the oceans. However, a serious problem diagnosed in the ERA-40 analyses is excessive tropical oceanic precipitation, particularly after 1991 (e.g., Trenberth et al. 2002; Uppala et al. 2005). This was due in part to effects of volcanic aerosols on high resolution infrared radiation sounder (HIRS) infrared radiances following the eruption of Mt. Pinatubo, which were not included directly in the forward radiative transfer model used in the variational analysis. This also occurred just at the time NOAA-12 became operational thereby affecting the bias correction. Inadequately corrected infrared radiance biases tend to result in spurious humidity changes in the tropical troposphere, since the relatively low background errors specified for temperature force analysis changes predominantly in humidity. An initial poor bias correction of SSM/I data was corrected for ERA-40 analyses from January 1993, along with revised thinning, channel-selection and quality control of HIRS radiances in 1997 and prior to 1989. [This peculiar sequence comes from the fact that there were multiple streams of reanalysis and that the pre-1989 stream was separate from the post-1989 stream].

We choose to focus on the ocean domain for the core analysis. We first performed an EOF analysis of each dataset independently. Although the EOF patterns and associated principle component time series were similar, they were also different enough to require a means of analyzing them together, which was initially accomplished through an extended combined EOF analysis. A coarse grid (every fourth point at T63 resolution) was chosen and all fields were concatenated and analyzed simultaneously. The resulting principle component time series was then projected onto the full grids, including over the land where data are available. The fields analyzed were the covariances. Hence, all fields contribute equally in determining the results and the emphasis is on the actual anomalies. However, while the results of this analysis were useful to us in the evaluation, it has become apparent that all datasets have major problems except perhaps the RSS SSM/I. Therefore, the main results shown will use the latter to define core time series and principle components.

Other approaches have also been tried. For instance, a singular value decomposition (SVD) analysis would effectively analyze the correlations and thus normalized anomalies, placing more weight on higher latitudes. Also, with five datasets, SVD analysis done pair-wise would result in ten different pairings. Alternative approaches would be to define the core time series in other ways, such as by choosing the Niño 3.4 sea surface temperature (SST) index, but this turns out to be unnecessary as the Niño 3.4 time series emerges from the analysis spontaneously.

3 Results

3.1 Comparisons of ERA-40 with Ross and Elliott

Because of the above-expressed concerns over ERA-40 water vapor fields, we have performed a detailed comparison with monthly means from Ross and Elliott (2001); referred to as RE. Separate sets of order 200 stations were used at both 0000 UTC and 1200 UTC, and our initial evaluation examined these separately; but results are combined for our presentation to give about 240 total stations. In each case, we extracted the

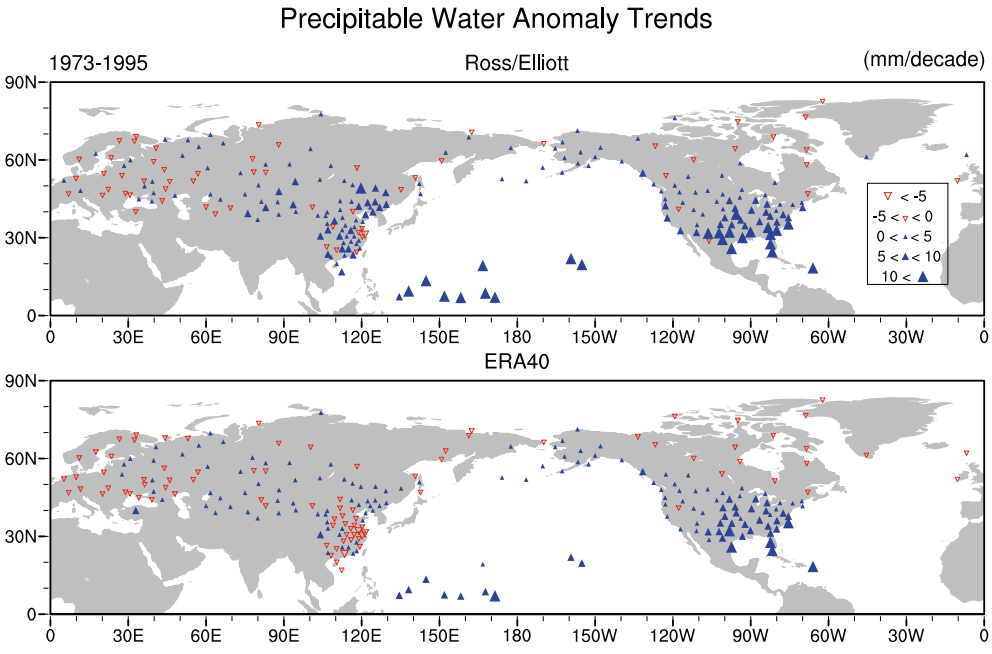

Fig. 1 Map showing the distribution of stations from Ross and Elliott (2001) and the linear trends from 1973 to 1996 for RE (*top*) and ERA-40 (*bottom*) in mm per decade. The apex on the *triangles* indicates whether the trend is up or down and the upward trends are also given by *solid triangles*

nearest grid point at T106 resolution from ERA-40 (1.125° grid) and masked the data to match the sonde data in the few cases in which some sonde data were missing.

Figure 1 presents the map of stations along with the trends, which we return to shortly. Several other basic statistics for monthly means from 1973 through 1995 are of interest at first. To summarize a large number of comparisons, the stations have been stratified by latitude (Fig. 2). The first panel of Fig. 2 gives the standard deviation of the monthly mean anomalies as a measure of the signal of the variability. Here, the variances from ERA-40 and RE are averaged, as they are fairly similar, and the square root taken. Standard deviations peak at 3.5 mm in the tropics and drop down to about 1 mm at high latitudes. In the tropics and subtropics, a lot of the variability is ENSO related. The second panel presents the correlations between the anomalies at each station, and values are uniformly high except at one station. The 10th percentile is 0.86, the 90th percentile is 0.97, and the median correlation is 0.94. Another measure of agreement is in the third panel, which shows the ratio of the rms differences to the standard deviation as a percentage. The rms differences also drop off at higher latitudes and are mostly less than 1 mm outside of the tropics. The two high values near 40°N are associated with low standard deviations. The 10th and 90th percentiles are 25% and 55%, and the median rms difference is 36% of

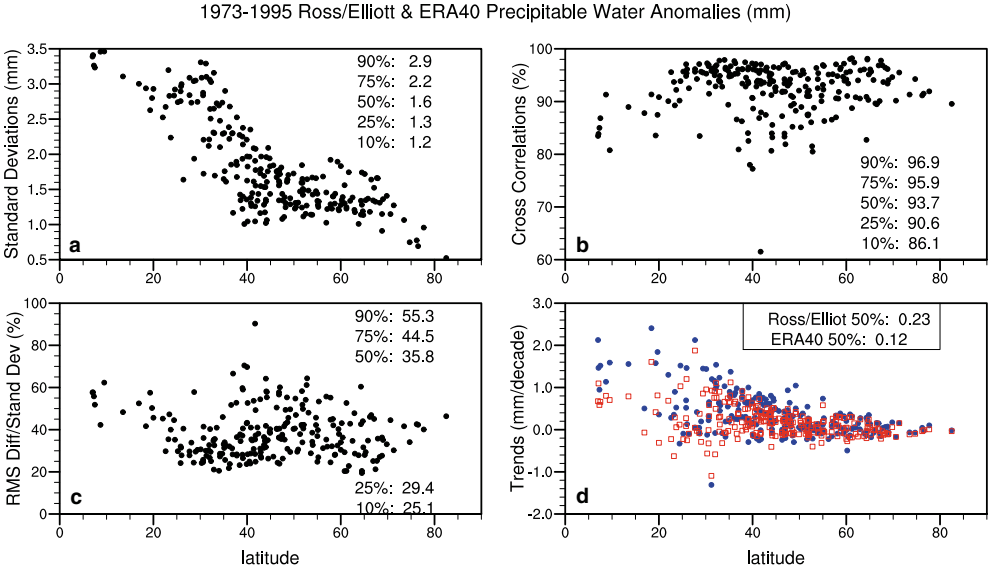

Fig. 2 Results for the RE station locations for 1973–1995 as a function of latitude. **a** standard deviation of monthly anomalies (based on average variances) in mm. **b** correlations as %. **c** Ratio of the rms difference to the standard deviation in %. **d** Linear trends, where the RE trends are given by closed circles and the ERA-40 trends are given by *open squares*, in mm per decade. Within each panel is given the 10th, 25th, 50th, 75th, and 90th percentiles, except the last panel has only the medians

the standard deviation. In general, the agreement is very good.

Some of the disagreement stems from slightly different trends, given in the fourth panel of Fig. 2 and also in Fig. 1. RE trends are generally greater than ERA-40 trends for this period. The 10th and 90th percentiles for RE versus ERA-40 are −0.13 versus −0.16 and 1.00 mm versus 0.69 mm per decade, while the median trends are 0.23 mm versus 0.12 mm per decade respectively . The tropical stations are mostly in the tropical Pacific (Fig. 1), and RE trends are greater than ERA-40 in all cases and at both 0000 UTC (ten stations) and 1200 UTC (four stations). Plots (not shown) reveal that the differences are greatest prior to 1979 when the TOVS satellite data was introduced. Agreement is quite good over southern USA but again the ERA-40 trends are somewhat less, particularly in the west. Over China, the ERA-40 trends are more similar to each other at different locations, and quite a bit less than RE. China is one area where ERA-40 made significant radiation bias corrections to radiosonde temperatures (Andrae et al. 2004). In both cases trends are small and insignificant over Europe.

Similar comparisons were made between RE and NVAP for the much shorter period from 1988–1995 (not shown). Results are generally very good at 90% of the stations: the 10th percentile correlation is 0.86 and the 90th percentile for rms differences relative to the standard deviation is 0.54, but the disagreements are quite large at a number of stations, including several over China, and the strong negative trends in NVAP at San Juan, Puerto Rico (18.4°N 66°W) appear to be wrong.

3.2 Comparisons with some updated sondes

To check on the veracity of some records, we have examined the 29 out of 94 U.S. stations that reported in 2000 whose sondes apparently did not change manufacturer in the 1990s (there may have been changes from VIZ-B to VIZ-B-2 to VIZ Microsonde, see Elliott et al. 2002). These came from the NCEP reanalysis archive, as assembled by Jack Woollen into monthly means for data through 1999. We used these to compute the precipitable water below 500 hPa. However, as only the standard level data were available for monthly means, the result is likely to be slightly biased relative to a computation based on daily data at all significant levels. We therefore used the last 2 years of the RE data, 1994–1995, as an overlap period to transfer the record to the Woollen dataset. We then excluded stations with a lot of missing data and selected only stations in coastal regions to allow comparisons with SSM/I data at the nearest datapoint (we noted a few near-coastal points contaminated by land effects, and we avoided these). To quantify the comparisons among the products, we averaged the Woollen with RE data to create a record from 1973 to 1999, and compared that with ERA-40 at the station location, and ERA-40 with the SSM/I grid point value for 1988–2001, and then we plotted a band that straddles the two values.

The result is shown in Fig. 3 for six stations spread around the coast of the United States. This figure gives a good idea on how well the different data sets agree. The ERA-40 reanalysis should include the station data, but analyzed values are influenced by other regions, satellite data, and the model forecasts. They have the advantage of being complete, whereas a check on the Woollen sonde data for 1994–1995 indicates for the stations presented, that none had complete records, and the monthly means are not consistent in that some pressure levels have more values than others. For Oakland, CA, for the 24 months, days of data missing in a month included 22, 13, and 11 out of 30 or 31. Months at the six stations with more than 10% of data missing ranged from 4 (Key West, FL) to 15 (Quillayute, WA) out of 24. Clearly this is a source of error for the sonde data. At Oakland, the annual cycle was evidently anomalous during 1994–1995 and thus it appears in the anomalies in earlier years in all records.

Resulting statistics are given in Table 1. Standard deviations for both periods and locations are similar except at San Juan, Puerto Rico where they changed from 1.7 mm to 1.9 mm for SSM/I and ERA-40 (1988–2001) versus 2.3 mm to 2.6 mm for ERA-40 and the radiosonde (1973–1999), indicating a real change in variability for the different years. Rms differences between ERA-40 and the radiosondes for 1973–1999 range from 0.5 mm at Quillayute to 1.2 mm at San Juan but are mostly less for ERA-40 and SSM/I for 1988–2001. The correlations are all 0.85 or higher. In general, therefore, the agreement is very good, given that SSM/I and ERA-40 are not point values and that sampling differences exist.

3.3 Comparisons for 1988–2001

The main expansion of areal coverage with considerable confidence comes from the SSM/I data over the oceans. The chief focus of this article is on this period and on the intercomparison of the different datasets. To set the stage and highlight the issues, we begin by presenting large-scale domain averages for the globe, oceans and land. SSM/I applies only to the oceans, while the land should be covered by the conventional radiosondes. TOVS and ATOVS water vapor channels are also used, but in different ways, by some of the products.

Figure 4 presents the monthly anomalies and the linear trends for each of the analyses for the globe, oceans and land areas. The first point to note is that the time series from NCEP-1 and NCEP-2 are very similar, as are the trends. Given that they used the same data and the same processing of the data related to water vapor, this is not surprising. Further examination reveals that they are essentially the same for this field, and hence we

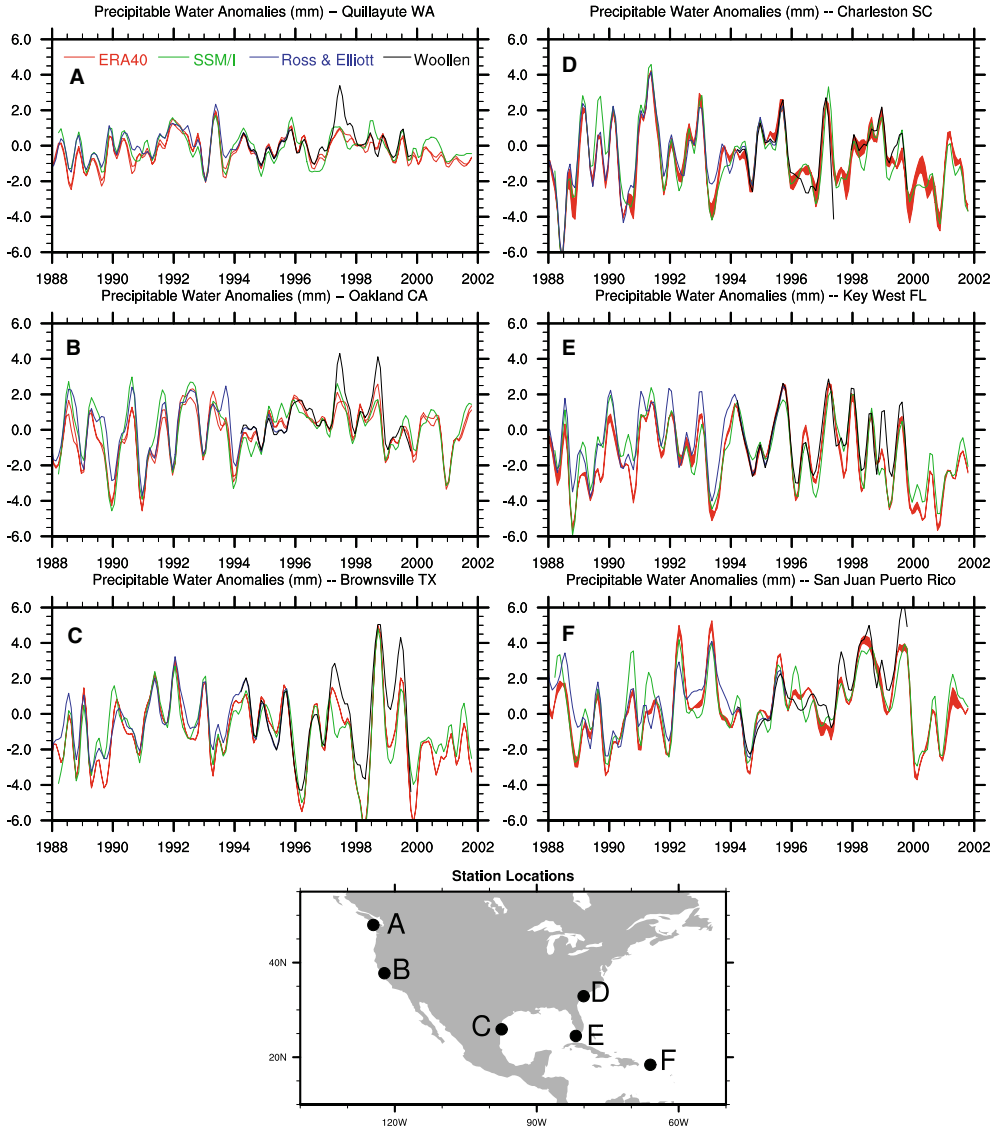

Fig. 3 Time series of monthly data smoothed with a 1-3-4-3-1 filter to reduce fluctuations less than 4 months period for the six locations around the coast of the United States from Ross and Elliott (2001) up till 1995, the Woollen sonde archive 1994–1999, the RSS SSM/I at the nearest grid point, and the ERA-40 interpolated to the nearest SSM/I gridpoint and the station location as a band. The stations are *A* Quillayute WA, *B* Oakland CA, *C* Brownsville TX, *D* Charleston SC, *E* Key West FL, and *F* San Juan, Puerto Rico, as given in the *bottom panel*

will show only one of the NCEP products on further plots.

While first examining the land areas in Fig. 4, it can be seen that the NVAP product is an outlier by featuring strong low frequency variability or jumps: high values before 1989 and after about 1998. ERA-40 agrees quite well with NCEP-1 and NCEP-2. Over the oceans, large differences in the linear trends immediately stand out. Positive trends of 0.7 mm per decade for ERA-40 contrast with negative trends of −0.1 mm per decade for NVAP, NCEP-1 and NCEP-2, with SSM/I from RSS in between showing positive trends of 0.37 mm per decade.

Table 1 Statistics of variability and agreement at or near the six U.S. radiosonde stations given in Fig. 3 by the letters

Map identifier	Station	Standard deviation (mm)	Rms differences (mm)		Correlations (%)	
			Sonde 1973–1999	SSM/I 1988–2001	Sonde 1973–1999	SSM/I 1988–2001
A	Quillayute	0.8	0.5	0.5	89	85
B	Oakland	1.4–1.5	0.9	0.6	87	93
C	Brownsville	1.8–2.0	0.9	0.8	91	93
D	Charleston	1.9–2.0	0.6	0.7	96	93
E	Key West	1.8–2.0	1.0	0.8	90	92
F	San Juan	1.7–2.6[a]	1.2	0.7	88	93

Separate statistics were computed for 1973–1999 for sondes versus ERA-40 and 1988–2001 for SSM/I versus ERA-40. The four values of standard deviation were similar except for San Juan[a] where the range was 1.7–1.9 mm for 1973–1999 and 2.3–2.6 mm for 1988–2001

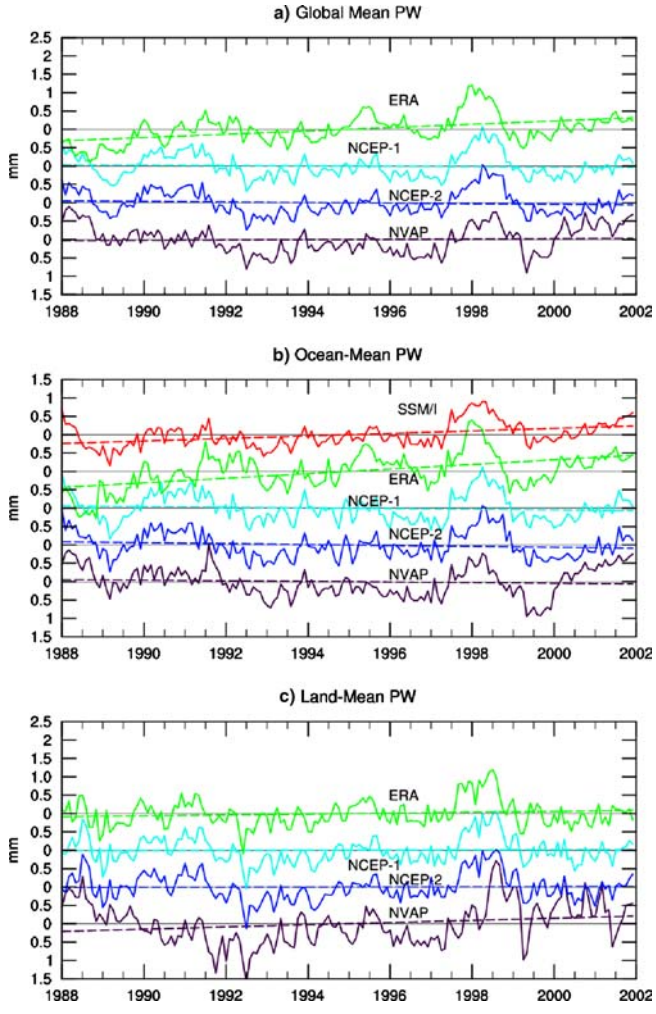

Fig. 4 Overall domain averages for the globe (*top*), ocean (*middle*) and land (*bottom*) of monthly anomalies from 1988 through 2001 and associated linear trends. Given are SSM/I, ERA-40, NCEP-1, NCEP-2, and NVAP. The mean annual cycle has been removed in each case

The Mount Pinatubo eruption in 1991 is followed by higher values from ERA-40. Again NVAP features large jumps at times, while in SSM/I fairly large negative excursions in 1988–1989 are offset by large positive excursions in 1997–1998. These features are somewhat common to all series, and relate to the 1988–1989 La Niña and 1997–1998 El Niño, i.e. they depict a real signal. The global values are dominated by the ocean values, as they constitute $>70\%$ of the domain.

The long-term average precipitable water fields are quite similar in general, with highest values exceeding 50 mm over the Warm Pool in the tropical western Pacific. The annual mean for ERA-40 (Fig. 5) is used to highlight the differences with other products. As previously found (Trenberth and Guillemot 1998), the NCEP fields are much less where values are large and too high in subtropical anticyclones (notably the South Pacific High) where values should be low. These NCEP biases also apply relative to SSM/I. NVAP mean fields are somewhat lower in the Warm Pool region and across the tropical Indian Ocean, but quite a lot higher over the Sahara, Arabian Peninsula and Gobi desert, all are very dry but poorly observed regions (cf. Fig. 1). The SSM/I fields, over the oceans only, are quite similar but less by order 1 mm or so in the tropics. Similar results were found by Allan et al. (2004). Possibly SSM/I values are biased slightly low by having to exclude heavy rainfall events, but it is likely that ERA-40 values are biased high, as discussed elsewhere here. SSM/I also features higher values over sea ice regions in both hemispheres. Precipitable water cannot be retrieved over sea-ice and differences may arise from different masking and sampling.

Taking the monthly anomalies and computing standard deviations (Fig. 6) reveals the high variability for ERA-40 (in the top panel as a reference) in the Pacific, associated with ENSO, and in the regions of the convergence zones over the oceans and northern Australia. NCEP variability is much less and deficient (Trenberth and Guillemot 1998). NVAP variability is quite similar to ERA-40 overall except that high mountain areas (Himalayas, Andes, Greenland, Antarctica) stand out as problem areas where the NVAP product is much too high (owing to spurious variance, e.g., Fig. 7). Values are also higher over Africa. Over the oceans, SSM/I variability is slightly less than ERA-40, but with no strong structure, and may simply reflect the bias in the mean values.

To further examine the variability, Fig. 7 presents some differences in anomalies of zonal averages as latitude-time sections. Here, we see that the differences are not systematic but vary with time. The abrupt differences between SSM/I and NVAP, especially at the end of 1992 and 1999, are both the times of major changes in procedures in processing NVAP; see Sect. 2. Hence this figure highlights one set of problems with NVAP. ERA-40 anomalies are much larger relative to NVAP and SSM/I in 1991–1992 and 1995–1996 in particular, and slightly larger than NVAP for 1989–1999. This is a bit misleading, as in absolute terms, the ERA-40 and SSM/I values agree best before 1989 and ERA-40 values are spuriously higher after that time, but this mean difference is removed in forming anomalies. The revised procedures in ERA-40 in 1997 and before 1989 are evidently the source of the improved agreement with other products after 1997, but it is only a relative improvement, as the total values remain high. It seems likely that the resurgent large ERA-40 values in 1995–1996 are associated with the loss of the NOAA-11 satellite at the end of 1994 and the new data that came in from NOAA-14 a few months into 1995. Hence, the bias correction of NOAA-14 was relative to just one satellite, NOAA-12, which had been influenced by the Pinatubo eruption.

Figure 8 further shows correlations among some of the products for monthly anomalies from 1988 to 2001. For ERA-40 and SSM/I, the correlations are mostly

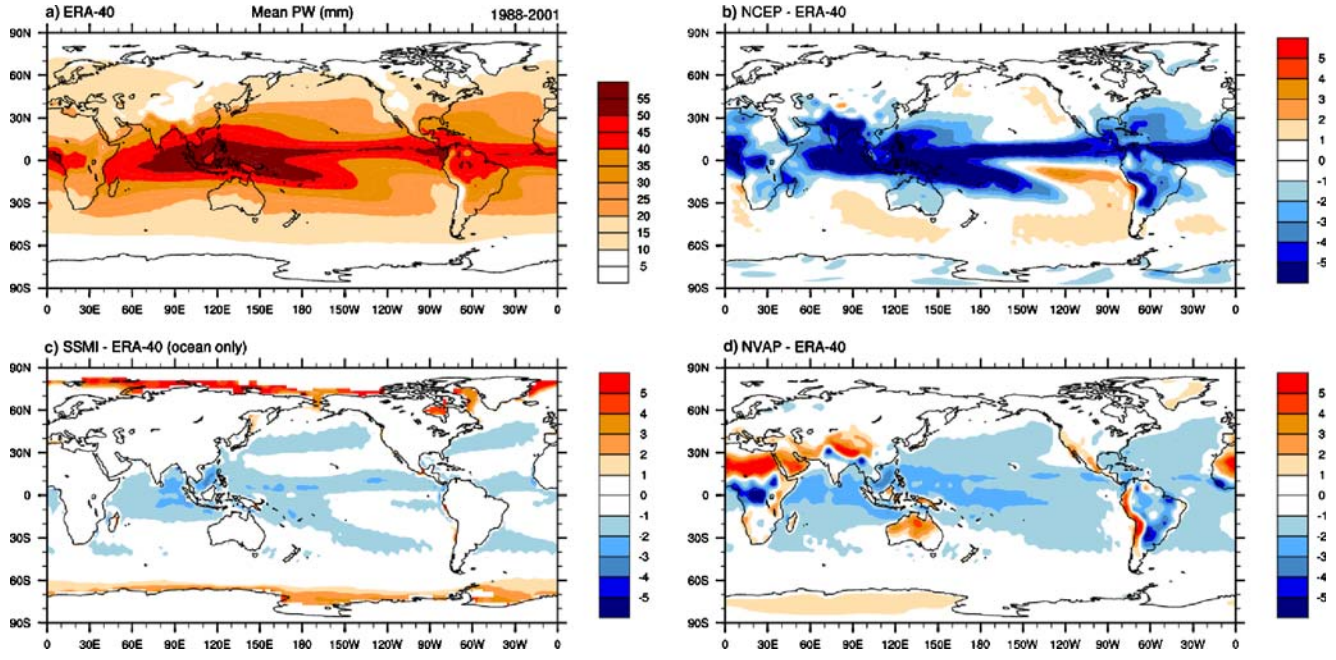

Fig. 5 Annual averages of precipitable water for 1988–2001 (mm) from ERA-40 and differences with NCEP, SSM/I and NVAP

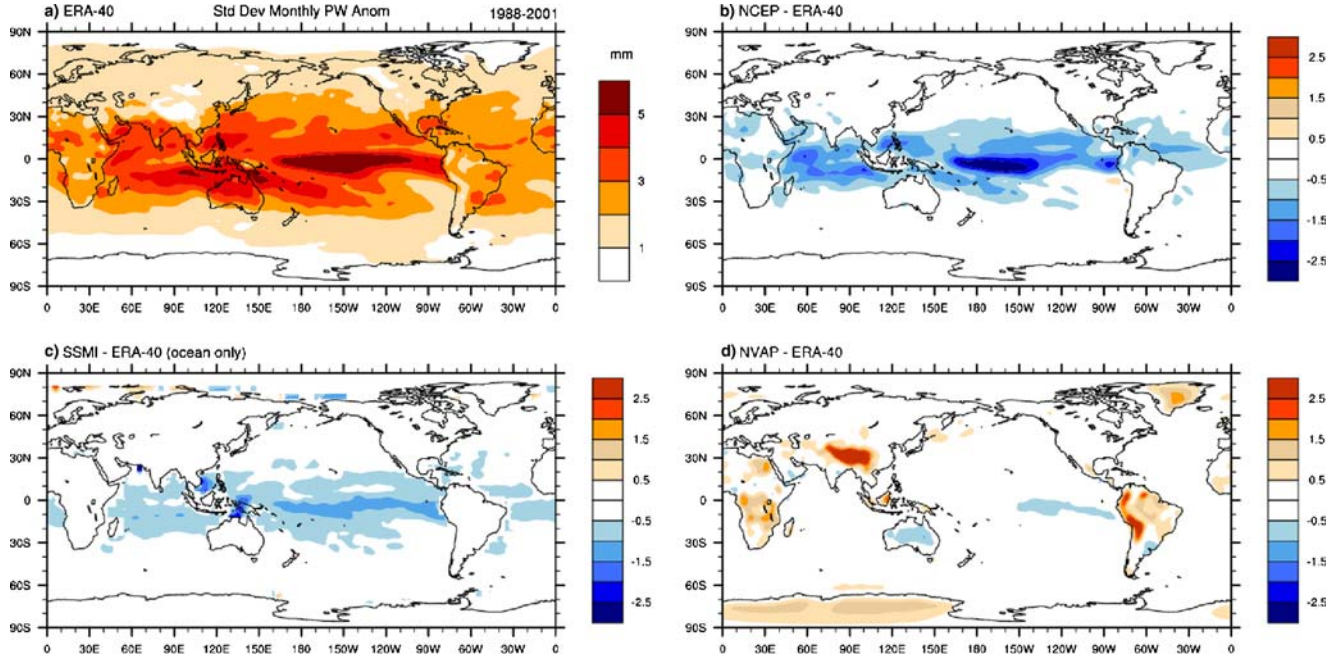

Fig. 6 Standard deviation of precipitable water monthly anomalies from ERA-40 for 1988–2001, and differences with NCEP, SSM/I and NVAP

over 0.9, and are especially strong in the Pacific inter tropical convergence zone (ITCZ) and South Pacific convergence zone (SPCZ) regions that are greatly impacted by ENSO. Lower correlations of order 0.85 are found in some midlatitude storm track regions. Correlations between ERA-40 and NVAP are generally high and similar in magnitude to those with SSM/I over the oceans, but values drop below 0.5 over many parts of the land, in particular those areas with missing data in Fig. 1 and with high elevations. This includes much of the Southern Hemisphere land except for Australia. Whereas the ERA-40 analysis has full accounting of the mountain topography, such as the Himalayas and Andes, the NVAP analysis does not, and interpolation of TOVS retrievals into these regions is a source of problems (Trenberth and Guillemot 1995).

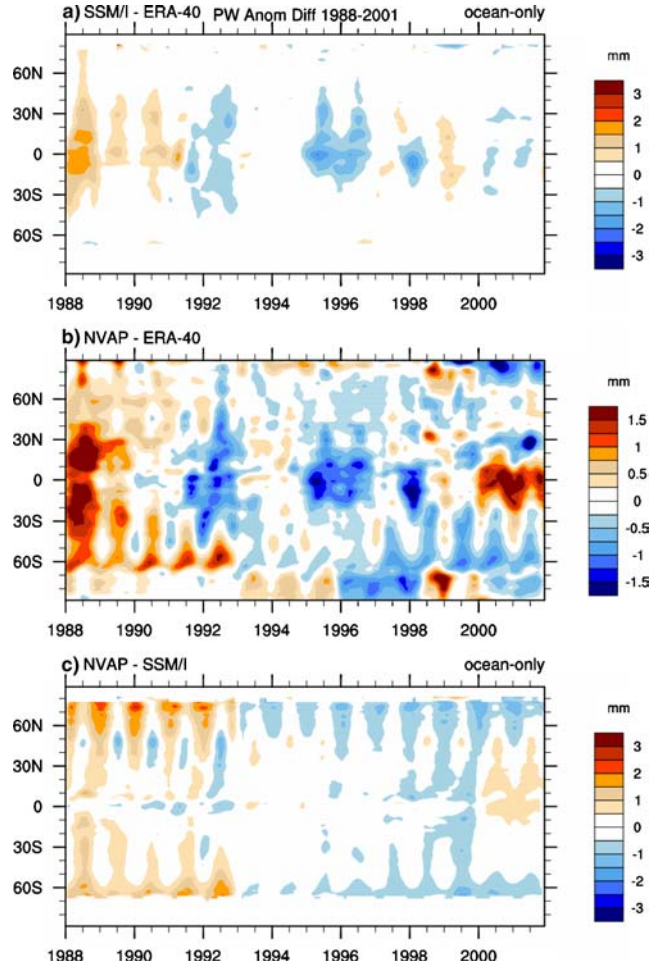

Fig. 7 Latitude-time series for 1988–2001 of anomalies of zonal mean differences between ERA-40 and SSM/I for the oceans (*top*) and NVAP globally (*middle*), and between NVAP and SSM/I for the oceans (*bottom*) in mm

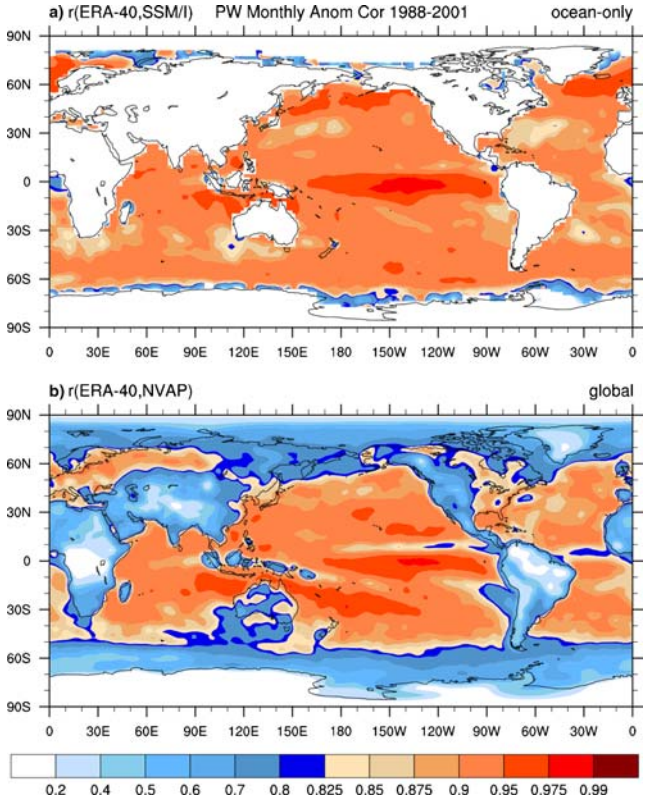

Fig. 8 Correlations of monthly anomalies of precipitable water between ERA-40 and SSM/I (*top*) and NVAP (*bottom*) for 1988 to 2001

As noted in the introduction, trends in water vapor are of considerable interest but are perhaps the most challenging to obtain with reliability. Maps of linear trends (Fig. 9) reveal similarities in the gross patterns, suggesting an influence of ENSO in the Pacific. NVAP linear trends are exaggerated where they agree with others, but strong negative trends are evident over the southern oceans and land areas with poor data, including northern Africa and southern Asia. The NCEP trends are more negative than others in most places, although the patterns appear related. Closer examination reveals that the main discrepancies are over the oceans. There is quite good agreement between ERA-40 and NCEP over most land areas except Africa, i.e. in areas where values are controlled by radiosondes.

From the above, it is clear that, aside from SSM/I, there appear to be substantial problems in all the other datasets with regard to trends and low frequency variability over the oceans. The linear trends from 1988 to 2001 based on SSM/I over the oceans (Fig. 4) show overall positive trends of 0.37 mm per decade or about 1.3% per decade. Fairly large negative excursions in 1988–1989 perhaps associated with the 1988–1989 La Niña, that are later followed by large positive excursions in 1997–1998 associated with the huge El Niño event, influence the linear trends somewhat. The spatial structure of the trends also suggests an ENSO influence. However, this association is complex and amplified in the Sect. 3.5.

3.4 SSM/I trends from 1988 to 2003

For RSS SSM/I, we can update the time period through 2003 (which was not possible for ERA-40 products) (Figs. 10, 11) and the trends are somewhat more uniform. The linear trend over the oceans as a whole is 0.41 mm per decade or about 1.3% per decade. The normalization to get percentage trends was done by the local monthly mean, and then these were averaged to get the area mean, so there is no simple conversion factor. Hence, the two Figs. 10 and 11 complement each other and give different perspectives on the trends. Figure 10 emphasizes the tropics while in Fig. 11 the response is more uniformly distributed over the oceans, and accentuated near sea-ice changes in the North Atlantic. The time series are very similar (correlation 0.93). Extending the record by 2 years has somewhat diminished the ENSO imprint on the pat-

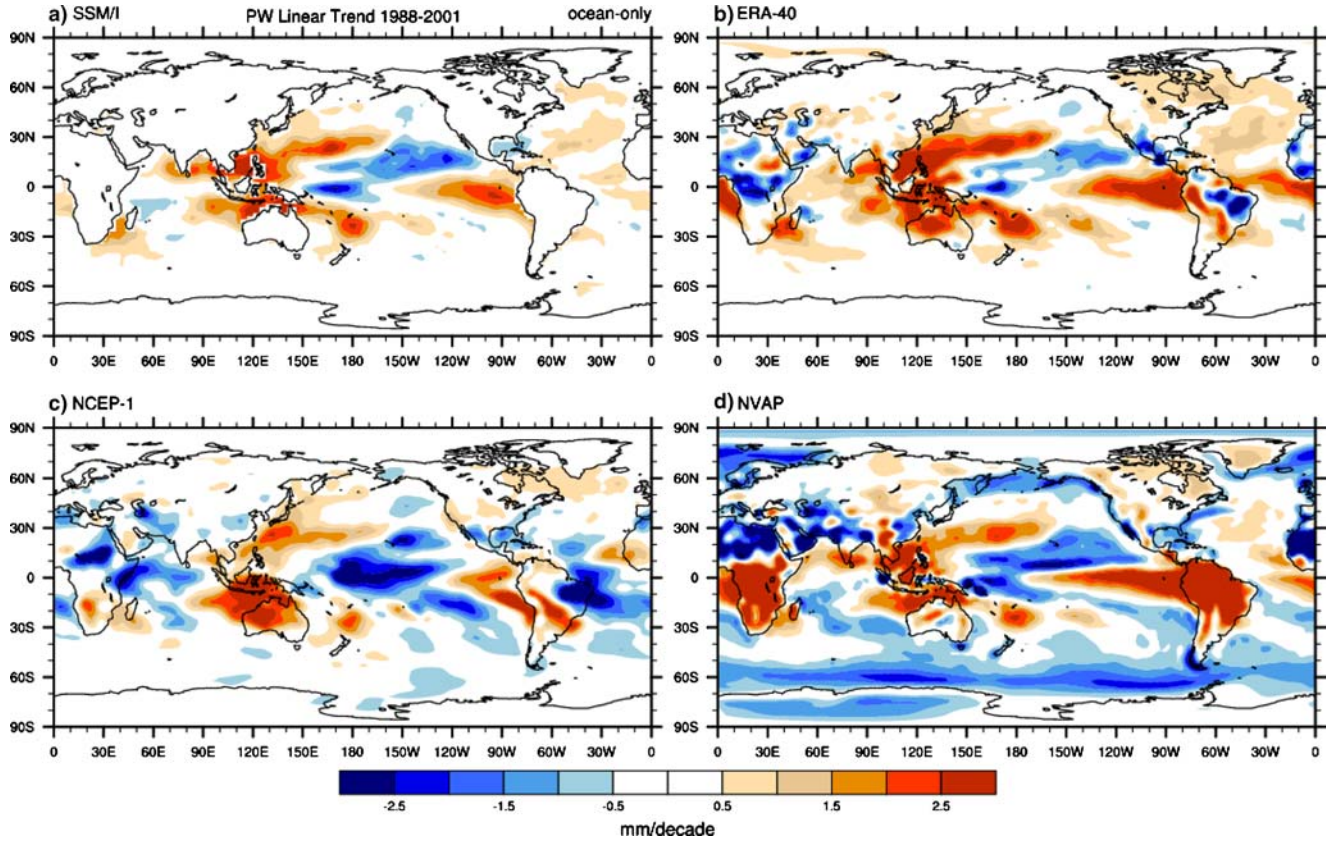

Fig. 9 Linear trend in mm per decade of the SSM/I (ocean only), ERA-40, NCEP-1 and NVAP fields for 1988–2001

terns and trends and the spatial average over the whole oceans is clearly more robust than local values. Increases in precipitable water are widespread over the Indian and Atlantic oceans.

We have tested the significance of the trend using two methods based on Monte Carlo techniques. Generating 10,000 series of annual means by selecting elements from the original time series at random, the observed trend is significant at the 99.67th percentile. Alternatively, based on the selection of annual differences, which are not correlated at all from year to year and which allow for a persisting random walk of the data, the trend lies at the 96th percentile of this distribution. If we assess the 95% confidence level based on sampling, then the error bars in the linear trend are ± 0.08 mm per decade.

This does not address uncertainties in the handoff of the signal from one satellite to the next, and we have examined the statistics of the overlaps between different satellites. Differences exist because of changes in data coverage, editing of the data, and so on. Differences between F10 and F11 are stable for 5 years until the last year of F10 data in 1997, when the differences jump by about 0.06 mm. Of more concern are differences between F11 and F13, which apparently jumped by about 0.08 mm for 1999–2000 relative to 1995–1998. Similarly differences between F13 and F14 are stable for about 6 years but have an offset in 2003 of order 0.1 mm, although F15 supports the F13 values. By generating sets of time series with different permutations in terms of the mixes of available satellites, we can assess how much these alter the overall trends. There are nine possible ways to generate time series from 1988 through 2003. The lowest linear trend was 0.380 mm per decade, the highest was 0.430 mm per decade, and both the median and the mean were 0.398 mm per decade, which is slightly lower than the case where all satellites are combined. If we interpret this range as about the 10th to 90th percentiles, given nine values, then the 95% confidence limits are ± 0.03 mm per decade, assuming a Gaussian distribution.

Combining the two errors, gives an overall trend as 0.40 ± 0.09 mm per decade, where these are 95% confidence limits. In terms of percent, which places more emphasis on higher latitude trends, the trend is $1.28 \pm 0.29\%$ per decade, which we round to $1.3 \pm 0.3\%$ per decade.

Much of the pattern of trends can be explained by the observed SST trends over the same period. Wentz and Schabel (2000) find, for a much shorter period, that the regression coefficient is 9.2% K^{-1} . We find the best value for the time series from 30°N to 30°S is 7.83 $\pm 0.1\%$ K^{-1} (correlation 0.87) for 1988–2003 or 8.87% K^{-1} for the global ocean (correlation 0.84), see Fig. 12. Both correlations are highly statistically significant. The

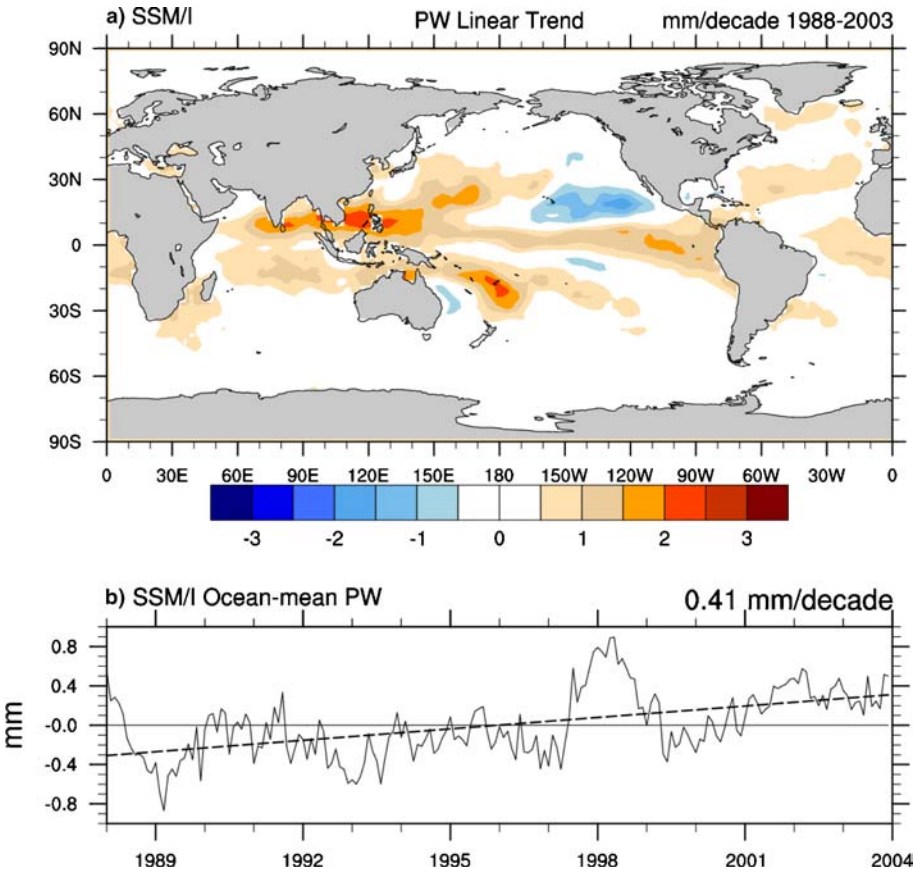

Fig. 10 Linear trend in precipitable water for 1988–2003 in mm per decade and the time series for the integral over the global ocean, which has a linear trend of 0.41 mm per decade

spatial correlation between the fields in Figs. 11 and 12 for 1988–2003 is 0.60 for 30°N to 30°S and 0.65 over the global oceans, both statistically significant at the 5% and 1% levels. The regression values are very close to the 7% K^{-1} expected from Clausius–Clapeyron equation for the water-holding capacity of the atmosphere, but are presumably slightly larger owing to the amplification associated with air temperature versus SST (especially with altitude in the tropics associated with the moist adiabatic lapse rate). Cooling of SSTs and negative trends in precipitable water are apparent over the central subtropical Pacific, including the Hawaiian Islands area, and extending northwards. One discrepancy is in the Gulf of Mexico, where SSTs have risen but precipitable water appears to have decreased slightly. These decreases are seen in Fig. 3, where the large drop in values in 1999 at Brownsville, Key West and San Juan in SSM/I is verified by the ERA-40 data, resulting in slight negative linear trends at the first two stations. However, the negative trend of −1.0 mm per decade for 1988–2001 at Key West becomes a positive trend of +1.3 mm per decade for the radiosonde data over the longer period 1973–1999, and with similar results at the other stations. Generally, Fig. 3 provides further confidence that the trends in SSM/I data are reliable.

As we discuss below, precipitable water is not only related to SST, however, but is also clearly linked to moisture transport and precipitation; in the tropics, the patterns of precipitation variability are strongly linked to ENSO and SST variability.

3.5 EOF analysis

Only the ocean domain was used to define the results of the analysis and regression is used to extend the results over land. The problems revealed in NCEP, NVAP and ERA-40 limit the value of the results of the extended EOF analysis of all datasets combined, and instead we have decided to present the first three EOFs from SSM/I, along with the associated patterns and variance accounted for in the other datasets.

The first EOF (Fig. 13) accounts for 19% of the SSM/I variance over the ocean and is strongly related to ENSO during this period. The time series is highly correlated with Niño 3.4 SST anomalies at 0.92. It exhibits no trend of any consequence and actually has a slight negative contribution to the global ocean trend from Fig. 4 of −0.02 mm per decade. The pattern is identifiable with the changes in precipitation and SST in the tropics associated with ENSO (Trenberth and Caron 2000) in all fields, except for NCEP, which is not as well defined. The variances accounted for by the patterns for each datasets are also given above each plot, firstly for the global ocean domain (and therefore comparable to the value for SSM/I), and secondly for the global

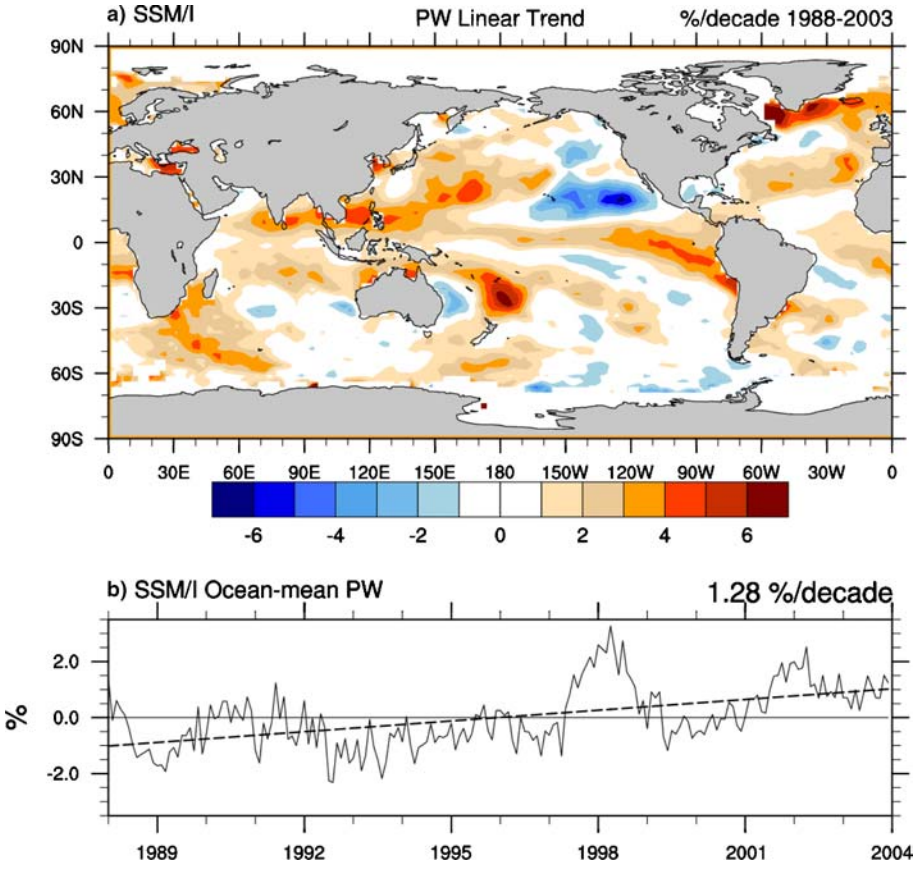

Fig. 11 Linear trend in precipitable water for 1988–2003 in % per decade and the time series for the integral over the global ocean, which has a linear trend of 1.3 mm per decade

domain. For the NCEP reanalyses, the latter is lowest of the datasets (10.4%), while for ERA-40 the value is 13.2%, similar to NVAP 13.1%.

The second EOF (Fig. 14), which accounts for 9.1% of the monthly SSM/I variance, is also related to ENSO. The dominant signature extends from the maritime continent of Indonesia across the Pacific, but with most of its amplitude occurring during 1998. It relates especially to the exceptional nature of the 1997–1998 El Niño event in which convection extended all the way across the Pacific along the equator early in 1998, leaving a much drier region over and south of Hawaii from the dateline to the Caribbean. It is this strange pattern that accounts for more of the linear trend for the global ocean than any other EOF. For the average over the entire ocean this EOF accounts for 0.17 mm per decade of the trend in Fig. 4 for SSM/I (46% of the total). The similarity of the spatial structures between Figs. 14 and

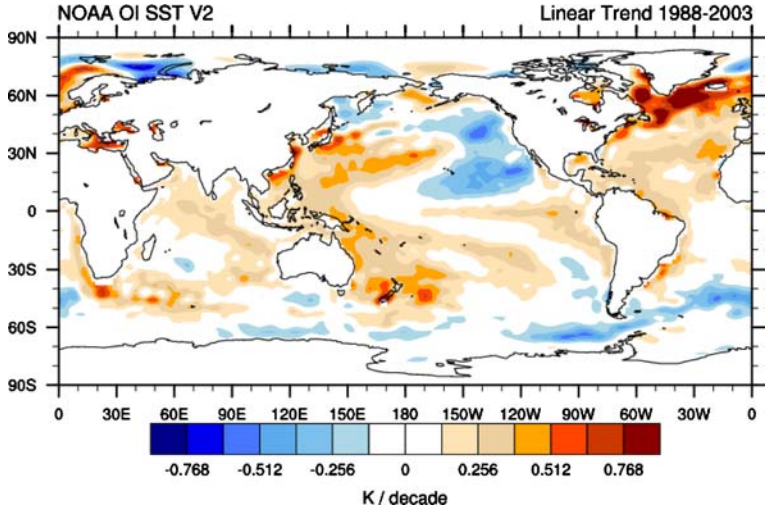

Fig. 12 Linear trend of SST 1988–2003. The color key is chosen to match the expected change in precipitable water from regression from 30°N to 30°S of 7.8% K^{-1} in Fig. 11

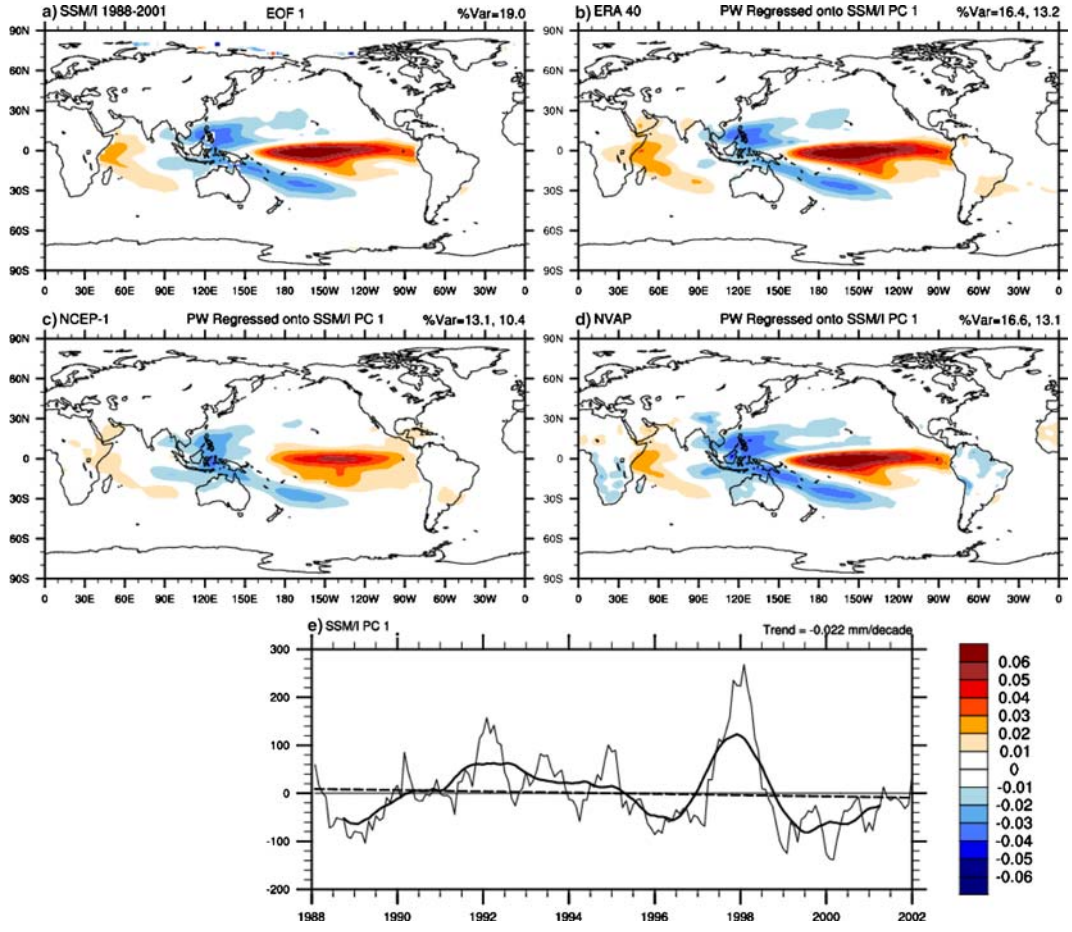

Fig. 13 SSM/I EOF first mode, which explains 19.0% of the variance overall. The principle component time series is given below, and the regression patterns for ERA-40, NCEP-1 and NVAP are given in the other three panels, with the percent variance accounted for above each panel for the global oceans and globe, respectively. The *heavy line* indicates an 18 month running mean.

9 is also clear. The pattern is strong and clear in both ERA-40 and NVAP, and weakest in NCEP. This also helps account for why the trends in NCEP are much smaller.

EOF 3 (Fig. 15) also accounts for some of the linear trend over the oceans (0.06 mm per decade) and again has strongest fluctuations around the time of the 1997–1998 El Niño event, although the weaker El Niño of 1992 is also represented. From this pattern, values of precipitable water are trending higher in the near equatorial regions across the Indian and Pacific oceans, over southern Africa and South America. The NVAP pattern is quite good over the oceans but extends into Africa and South America much more so than ERA-40 and NCEP. Once again the NCEP patterns are least realistic.

4 Discussion and conclusions

It is evident that the analysis of precipitable water variability is dominated by the evolution of ENSO and especially the structures that occurred during and following the 1997–1998 El Niño event. More generally, the links of precipitable water variations with ENSO serve to highlight the strong relationships over the oceans of precipitable water with SSTs and changes in tropical precipitation, as the ITCZ, SPCZ, and monsoon troughs vary. In fact the relationship is strong both in terms of the spatial structure and temporal variability. Careful comparisons of EOF-1 (Fig. 14) with ENSO patterns of SST and rainfall suggest that the relationship may be stronger with the latter in the tropics. While positive SST anomalies tend to be associated with higher rainfalls, the structure of rainfall changes is greatly influenced by climatological features, such as the ITCZ and SPCZ, and their movement, and this allows for some discrimination to be discerned in terms of the relationship with precipitable water variability. The link between precipitable water and rainfall is not surprising, as both are closely associated with the mean flow and convergence of moisture by the trade winds in the tropics, while the latter is in turn linked to SST patterns. Free running atmospheric climate models forced with observed SSTs similarly reproduce observed

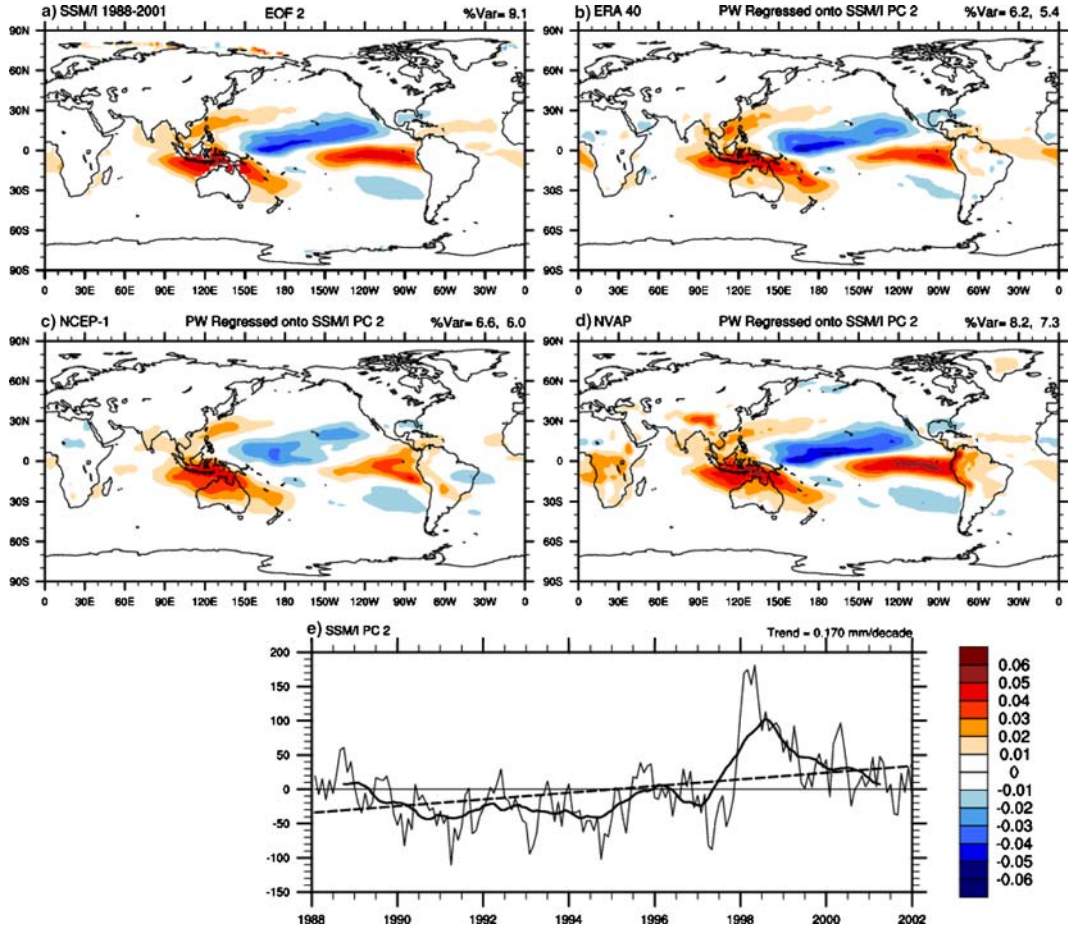

Fig. 14 SSM/I EOF second mode, which explains 9.1% of the variance overall. The principle component time series is given below, and the regression patterns for ERA-40, NCEP-1 and NVAP are given in the other three panels, with the percent variance accounted for above each panel for the global oceans and globe, respectively. The *heavy line* indicates an 18 month running mean.

changes in water vapor and their relationships with SSTs (e.g., Soden 2000).

The dominance of the 1997–1998 El Niño event in the record suggests that a longer time series may be required to obtain fully stable patterns of trends, although it also suggests that the main variability might be deduced from past SST and associated precipitation variations. The linear trends from 1988 to 2001 versus 1988 to 2003 indicate more widespread increases as the period expands and the global ocean trend is much more robust and stable as data are added. Moreover, the main patterns of variability are robust across all the datasets, although the linear trend accounts for different portions of the total variance. One reason relates to the mean and variability fields as a whole, but another relates to the spurious variance present, especially in NVAP.

The main region where positive trends were not evident in the earlier analysis of Ross and Elliott (2001) using data for 1973 through 1995 was over Europe, and this also appears to be the case from 1988 to 2001 based on ERA-40 data in spite of large and positive trends over the North Atlantic in both SSM/I and ERA-40 data. This is also in spite of generally increasing trends in precipitation (IPCC 2001) in Europe and other mid-latitude regions. However, Philipona and Dürr (2004) find increases in surface humidity since 1981, and increases in water vapor and downward longwave radiation are present in central Europe from 1995 through 2003. The large positive trends from 1973 to 1995 over the United States (Fig. 1) in precipitable water appear to have slowed and even reversed slightly in the south, although increases continue along the West Coast (in ERA-40 and NCEP, Fig. 9) and have picked up in much of Canada. More intense rains have been observed in the U.S. (Groisman et al. 2004).

The evidence suggests that recent trends in precipitable water over the oceans are generally positive. This may be best measured by the global ocean average, which averages out the large regional effects of opposite sign associated with ENSO. The upward trends in moisture may form a partial explanation for the general positive trends in low and total cloudiness over the ocean (Norris 1999). We assess the global ocean trends from 1988 to 2003 to be 0.40 ± 0.09 mm per decade,

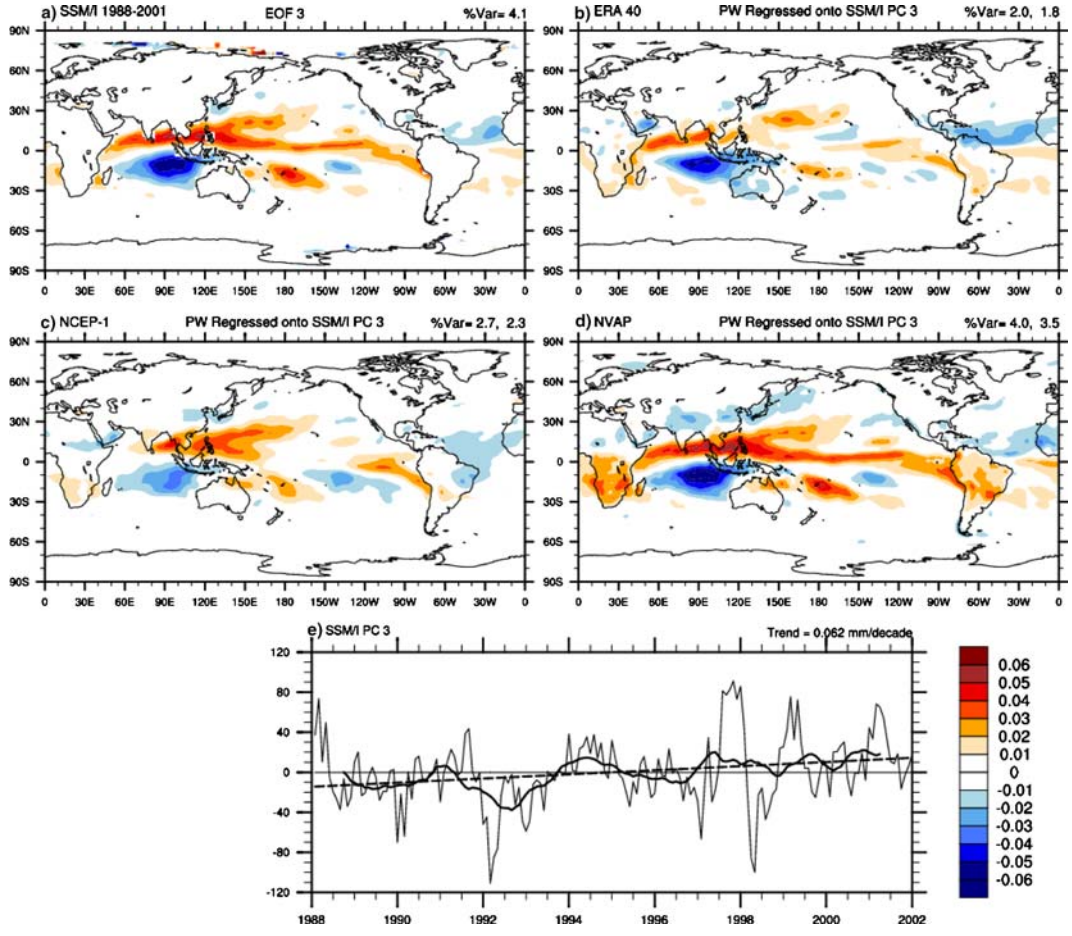

Fig. 15 SSM/I EOF third mode, which explains 4.1% of the variance overall. The principle component time series is given below, and the regression patterns for ERA-40, NCEP-1 and NVAP are given in the other three panels, with the percent variance accounted for above each panel for the global oceans and globe, respectively. The *heavy line* indicates an 18 month running mean.

where these are 95% confidence limits. In terms of percent, which places the emphasis more uniformly with latitude, the trend is $1.3 \pm 0.3\%$ per decade.

Precipitable water is a very important variable for climate, as discussed in the introduction, but the quality of most of the global analyses of this quantity leaves a great deal to be desired.

- Both NCEP reanalyses are deficient over the oceans in terms of the mean, the variability and trends, and the structures of variability are not very realistic. This stems from the lack of assimilation of water vapor information from satellites into the analyses and model biases. They agree reasonably well with ERA-40 over land where values are constrained by radiosondes, with some discrepancies over Africa.
- The NVAP dataset suffers from major changes in processing at the beginning of 1993 and 2000 that upsets analysis of trends and variability. Further, there are major problems in mountain areas and in regions where radiosonde data are not prevalent and TOVS data from the oceans are erroneously extended over land.
- The ERA-40 dataset appears to be quite reliable over land and where radiosondes exist, but suffers from substantial problems over the oceans, especially with values too high for 2 years following the Mount Pinatubo eruption in 1991 and again in 1995–1996, associated with problematic bias corrections of new satellites. The trends are generally not very reliable over the oceans. Allan et al. (2004) drew similar conclusions.
- The RSS SSM/I dataset appears to be realistic in terms of means, variability and trends over the oceans, although questions remain at high latitudes in areas frequented by sea ice. It is recommended that this dataset should be used for analyses of precipitable water and for model validation over the oceans from 1988 onwards.

Accordingly, great care should be taken by users of these data to factor in the known shortcomings in any analysis. The problems highlight the need for reprocessing of data, as has been done by RSS, and reanalyses that adequately take account of the changing observing system. This remains a major challenge.

Acknowledgements This research is partially sponsored by the NOAA CLIVAR and CCDD programs under grant NA17GP1376. The ERA-40 data used were provided by ECMWF. SSM/I data are produced by Remote Sensing Systems and sponsored by the NASA Earth Science REASoN DISCOVER Project. Data are available at http://www.remss.com. We thank Brian Soden and Adrian Simmons for comments.

References

Allan RP, Ringer MA, Pamment JA, Slingo A (2004) Simulation of the Earth's radiation budget by the European Centre for Medium-Range Weather Forecasts 40-year reanalysis (ERA40). J Geophys Res 109:D18107. DOI 10.1029/2004JD004816

Andrae U, Sokka N, Onogi K (2004) The radiosonde temperature bias corrections used in ERA-40. ERA-40 Project Report Series 15, 34 pp

Elliott WP, Gaffen DJ, (1991) On the utility of radiosonde archives for climate studies. Bull Amer Meteorol Soc 72:1507–1520

Elliott WP, Ross RJ, Blackmore WH (2002) Recent changes in NWS upper-air observations with emphasis on changes from VIZ to Vaisala radiosondes. Bull Amer Meteorol Soc 83:1003–1017

Greenwald TJ, Stephens GL, Von der Haar TH, Jackson DL (1993) A physical retrieval of cloud liquid water over the global oceans using SSM/I measurements. J Geophys Res 98:18471–18488

Ya GP, Knight RW, Karl TR, Easterling DR, Sun BM, Lawrimore JH (2004) Contemporary changes of the hydrological cycle over the contiguous United States: trends derived from in situ observations. J Hydrometeorol 5:64–85

Guichard F, Parsons D, Miller E (2000) Thermodynamic and radiative impact of the correction of sounding humidity bias in the tropics. J Climate 13:3611–3624

Held IM, Soden BJ (2000) Water vapor feedback and global warming. Ann Rev Energy Environ 25:441–475

Hense A, Krahe P, Flohn H (1988) Recent fluctuations of tropospheric temperature and water vapour content in the tropics. Meteorol Atmos Phys 38:215–227

IPCC (Intergovernmental Panel on Climate Change) (2001) Climate Change 2001. In: Houghton JT et al (eds) The scientific basis. Cambridge University Press, Cambridge, 881pp

Kalnay E, Kanamitsu M, Kistler R, Collins W, Deaven D, Gandin L, Iredell M, Saha S, White G, Woollen J, Zhu Y, Chelliah M, Ebisuzaki W, Higgins W, Janowiak J, Mo K-C, Ropelewski C, Leetmaa A, Reynolds R, Jenne R, Joseph D (1996) The NCEP/NCAR reanalysis project. Bull Amer Meteorol Soc 77:437–471

Kanamitsu M, Ebisuzaki W, Woolen J, Yang S-K, Hnilo JJ, Fiorino M, Potter GL (2002) NCEP-DOE AMIP-II reanalysis (R-2). Bull Amer Meteorol Soc 83:1631–1643

Kiehl JT, Trenberth KE (1997) Earth's annual global mean energy budget. Bull Amer Meteorol Soc 78:197–208

Lanzante JR, Klein SA, Seidel DJ (2003) Temporal homogenization of monthly radiosonde temperature data. Pt I: methodology. J Climate 16:224–240

Liu WT, Tang W, Wentz F (1992) Precipitable water and surface humidity over global oceans from Special Sensor Microwave Imager and European Centre for Medium Range Weather Forecasts. J Geophys Res 97:2251–2264

Marquart S, Ponater M, Mager F, Sausen R (2003) Future development of contrail cover, optical depth, and radiative forcing: impacts of increasing air traffic and climate change. J Climate 16:2890–2904

Norris JR (1999) On trends and possible artifacts in global ocean cloud cover between 1952 and 1995. J Climate 12:1864–1870

Philipona R, Dürr B (2004) Greenhouse forcing outweighs decreasing solar radiation driving rapid temperature rise over land. Geophys Res Lett 31:L22208. DOI:10.1029/2004GL020937

Randel DL, Vonder Haar TH, Ringerud MA, Stephens GL, Greenwald TJ, Combs CL (1996) A new global water vapor dataset. Bull Amer Meteorol Soc 77:1233–1246

Ross RJ, Elliott WP (1996) Tropospheric water vapor climatology and trends over North America: 1973–93. J Climate 9:3561–3574

Ross RJ, Elliott WP (2001) Radiosonde-based Northern Hemisphere tropospheric water vapor trends. J Climate 14:1602–1611

Simpson JJ, Berg JS, Koblinsky CJ, Hufford GL, Beckley B (2001) The NVAP global water vapor dataset: independent cross-comparison and multiyear variability. Remote Sensing Environ 76:112–129

Soden BJ (2000) The sensitivity of the tropical hydrological cycle to ENSO. J Climate 13:538–549

Soden BJ, Wetherald RT, Stenchikov GL, Robock A (2002) Global cooling after the eruption of Mount Pintubo: a test of climate feedback by water vapor. Science 296:727–730

Sohn B-J, Smith EA (2003) Explaining sources of discrepancy in SSM/I water vapor algorithms. J Climate 16:3229–3255

Trenberth KE (1995) Atmospheric circulation climate changes. Clim Change 31:427–453

Trenberth KE (1999) Atmospheric moisture recycling: role of advection and local evaporation. J Climate 12:1368–1381

Trenberth KE, Caron JM (2000) The southern oscillation revisited: sea level pressures, surface temperatures and precipitation. J Climate 13:4358–4365

Trenberth KE, Guillemot CJ (1995) Evaluation of the global atmospheric moisture budget as seen from analyses. J Climate 8:2255–2272

Trenberth KE, Guillemot CJ (1998) Evaluation of the atmospheric moisture and hydrological cycle in the NCEP/NCAR reanalyses. Clim Dyn 14:213–231

Trenberth KE, Smith L (2005) The mass of the atmosphere: a constraint on global analyses. J Climate 18:86–875

Trenberth KE, Stepaniak DP (2003a) Co-variability of components of poleward atmospheric energy transports on seasonal and interannual timescales. J Climate 16:3690–3704

Trenberth KE, Stepaniak DP (2003b) Seamless poleward atmospheric energy transports and implications for the Hadley circulation. J Climate 16:3705–3721

Trenberth KE, Stepaniak DP, Caron JM (2002) Preliminary evaluation of vertically-integrated fluxes of moisture and energy from ERA-40. Workshop on reanalysis. ECMWF, Reading, 5–9 November 2001. ERA-40 Proj Rep Ser 3:265–266

Trenberth KE, Dai A, Rasmussen RM, Parsons DB (2003) The changing character of precipitation. Bull Amer Meteorol Soc 84:1205–1217

Uppala SM, Kållberg PW, Simmons AJ, Andrae U, da Costa Bechtold V, Fiorino M, Gibson JK, Haseler J, Hernandez A, Kelly GA, Li X, Onogi K, Saarinen S, Sokka N, Allan RP, Andersson E, Arpe K, Balmaseda MA, Beljaars ACM, van de Berg L, Bidlot J, Bormann N, Caires S, Dethof A, Dragosavac M, Fisher M, Fuentes M, Hagemann S, Hólm E, Hoskins BJ, Isaksen L, Janssen PAEM, McNally AP, Mahfouf J-F, Jenne R, Morcrette J-J, Rayner NA, Saunders RW, Simon P, Sterl A, Trenberth KE, Untch A, Vasiljevic D, Viterbo P, Woollen J (2005) The ERA-40 reanalysis. Quart J Roy Meteor Soc (Submitted)

Von der Haar T et al (2003) Continuation of the NVAP global water vapor data sets for Pathfinder science analysis Science and Technology Corp. STC Technical Report 3333, 44 pp. http://eosweb.larc.nasa.gov/PRODOCS/nvap/sci_tech_report_3333.pdf

Wang J, Cole HL, Carlson DJ, Miller ER, Beierle K, Paukkunen A, Lane TK (2002) Corrections of humidity measurement errors from the Vaisala RS80 radiosonde—application to TOGA-COARE data. J Atmos Ocean Technol 19:981–1002

Wang J, Carlson DJ, Parsons DB, Hock TF, Lauritsen D, Cole HL, Beierle K, Chamberlain E (2003) Performance of operational radiosonde humidity sensors in direct comparison

with a chilled mirror dew-point hygrometer and its climate implication. Geophys Res Lett 30:1860. DOI 10.1029/2003GL016985

Wentz FJ (1997) A well-calibrated ocean algorithm for special sensor microwave/imager. J Geophys Res 102(C4):8703–8718. DOI 10.1029/96JC01751

Wentz FJ, Schabel M (2000) Precise climate monitoring using complementary satellite data sets. Nature 403:414–416

Zhai P, Eskridge RE (1997) Atmospheric water vapor over China. J Climate 10:2643–2652

Zveryaev II, Chu P-S (2003) Recent climate changes in precipitable water in the global tropics as revealed in National Centers for Environmental Prediction/National Center for Atmospheric Research reanalysis. J Geophys Res 108(D10):4311. DOI 10.1029/2002JD2476